

## FEDSM-ICNMM2010-' \$( +

### BLAST-INDUCED NEUROTRAUMA: CHARACTERIZING THE BLAST WAVE IMPACT AND TISSUE DEFORMATION

Jian Gao<sup>†</sup>, Sean Connell<sup>‡,£</sup>, Riya Shi<sup>‡,£</sup>, and Jun Chen<sup>†</sup>

<sup>†</sup>School of Mechanical Engineering

<sup>‡</sup>School of Biomedical Engineering

<sup>£</sup>Department of Basic Medical Sciences, School of Veterinary Medicine  
Purdue University  
West Lafayette, Indiana, 47907, U.S.A.

#### ABSTRACT

Primary blast injury, caused by exposure to the primary pressure wave emitted from explosive ordnance, is a common trauma associated with modern warfare activities. The central nervous system is particularly vulnerable to primary blast injury, which is responsible for many of the war related casualties and mortalities. An *ex vivo* model system is developed to introduce a blast wave, generated from a shock tube, directly to spinal cord tissue sample. A high-speed shadowgraphy is utilized to visualize the development of the blast wave and its interaction with the tissue samples. The surface deformation of the tissues is also measured for the analysis of internal stress and possible damage occurred in the tissue sample. Understanding the temporal development of the blast-tissue interaction provides valuable input for characterizing and modeling blast-induced neurotrauma. Particularly, tracking the sample surface deformation over time provides realistic boundary conditions for numerically simulating the injury and understanding the temporal development of stress.

#### INTRODUCTION

Primary blast injury (PBI), caused by exposure to the primary pressure wave generated by explosive devices, is a common injury modality associated with current war efforts. For instance, explosive blasts are responsible for approximately 65% of all combat injuries in modern war efforts. The prevalence of blast injury has steadily increased in the past decade due to rising levels of terrorist activity and has been termed the signature wound of the military in present day conflicts [1]. Specifically, PBI on the central nervous system, referred to as blast-induced neurotrauma (BINT), is a particularly prevalent injury and is responsible for many of the war related casualties and recurring disabilities of returning soldiers. Severe exposure can cause sudden death. However, even mild exposure can produce an initial acute injury marked by degraded neuronal function that elicits a secondary biochemical response, which further debases the injury site and impairs function [2, 3]. Long-term neurological disabilities of BINT include brain and spinal cord injury and degradation of rudimentary cognitive abilities that severing impairs the victim's quality of

life [4].

Despite the far-reaching detrimental effects of BINT, effective diagnostic and treatment protocols are nearly nonexistent because little is known about the injury mechanism. Previous attempts to understand BINT using animal models are mainly limited to the global response of blast injury, which is inadequate to decipher the physical injury mechanism at the tissue level. This is largely attributed to the models susceptibility to confounding systemic factors that mask or alter the neuronal response at the cellular level [5]. Alternative research efforts using *in vitro* cell culture models suffer a different set of problems. Isolated cell systems lack the local extracellular environment that likely affects neuronal behavior under stress [6, 7]. These factors will certainly influence the biomechanics of axons when the cord is deformed under blast loading. Consequently, isolated cell models yield a biologically irrelevant response to BINT. Therefore, sound understanding of the physical mechanism and modeling of BINT are paramount for appropriate diagnosis and treatment. Particularly, the rate and magnitude of tissue deformation is of imminent interest for calculating the internal stresses using a computational model and correlating these mechanical parameters to tissue damage to formulate accurate tissue failure criteria for BINT.

In this paper, we describe an experimental procedure to ascertain the physical characteristics of the blast wave, mechanical loading applied to the biological preparation, and resultant deformation of the tissue sample, by incorporating flow visualization techniques and *ex vivo* tissue tests. The work discussed here is part of on-going research activities aimed at modeling and characterizing BINT. Details about the experimental procedure are presented in the following section, followed by discussion of the preliminary results. The final section gives a summary and outlook.

## EXPERIMENTAL PROCEDURE

A schematic of the miniature *ex vivo* BINT model is shown in figure 1. In this setup, a repeatable primary blast injury is created on isolated sections of guinea pig spinal cord white matter.

### Blast Generation

The blast wave is generated from a 25mm-long shock tubing (NONEL Lead Line with an explosive lining of 0.1

grains/foot composed of tetranitramine (HMX) and aluminum), which is detonated by an electrical plasma discharge device (Wizard “ARC” Shock Tube Initiator) attached to a Mini Blasting Machine (Wizard 50G2). The explosive shock-wave is directed toward the tissue sample using a hollow blast nozzle which has an outer diameter of 6.4 mm and an inner diameter of 3.6 mm. Various degrees of blast intensity are created by varying the distance between the tube exit and the tissue sample. The nozzle is held vertically above the loading plate where the tissue sample is mounted. The data used in this paper is obtained from a blast nozzle of 80 mm long. A loading plate is placed beneath the blast nozzle, 14 mm from the nozzle exit, for mounting tissue samples. The development of blast wave structures, as well as the deformation of the tissue samples can be investigated. The free development of the blast wave can also be examined when the loading plate is removed.

### Tissue Sample Preparation

The spinal cord white matter tissue sample is prepared according to the procedure described in [8,9] and is approximately 10 mm×2.2 mm×2.2 mm in dimension. Adult female guinea pigs, weighing between 250 g and 350 g are deeply anesthetized. They are then transcardially perfused with cold oxygenated Krebs solution. The vertebral column is removed and the spinal cord ventral white matter is carefully excised by cutting through the pedicles longitudinally along the column. Prior to testing, the ventral white matter is allowed to recover and equilibrate in continuously oxygenated Krebs solution for at least one hour. The experimental protocol used for this study is approved by the Purdue University Animal Care and Use Committee. The tissue sample is placed on the loading plate in a way that its entire length (10 mm) fall into the field view of the camera, at a distance of 12 mm away from the nozzle exit to the sample top surface.

### Imaging Blast Wave and Tissue Deformation

Shadowgraph displays the light ray refraction resulted from optical inhomogeneities. The relative changes of light intensity in the plane of observation is proportional to the Laplacian of the refractive index  $n$ , i.e.,  $\Delta I/I \propto \nabla^2 n$ , where  $I$  is the light intensity [10, 11]. Particularly, the refractive

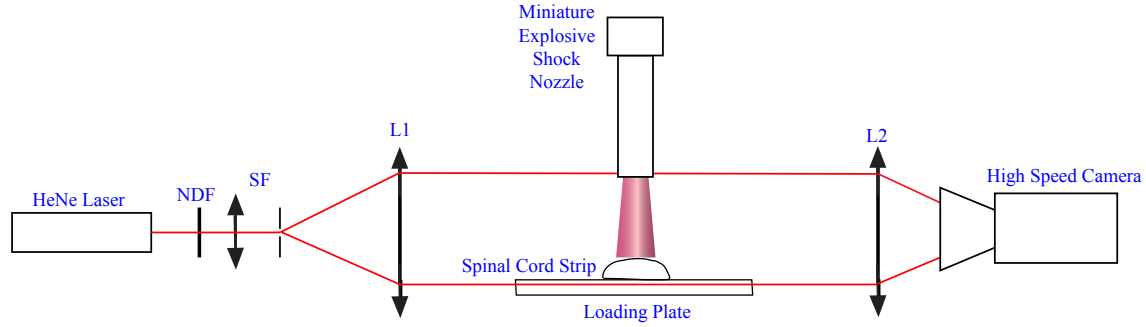


Figure 1. Schematic illustration of miniature *ex vivo* BINT model experiment. NDF: neutral density filter, SF: spatial filter, L1 and L2: a pair of collimating doublets, focal length  $f=200$  mm.

index of air is related to the density  $\rho$  by:

$$n = 1 + k\rho, \quad (1)$$

where constant  $k \sim 0.23 \text{ cm}^3/\text{g}$  [10]. Therefore, the shadowgraph is sensitive to changes of the second derivative of the gas density and it provides an effective visualization of flow field with large density variations. In the present work, a shadowgraph system is developed to record the development of the wavefront and structures associated with density changes caused by the blast wave.

A high-speed imaging system is developed to visualize the development of the blast wave as well as the deformation of the tissue sample, as shown in figure 1. Light from a continuous 15 mW He-Ne laser is attenuated (using a neutral density filter), spatially filtered, expanded and collimated, and then directed to the imaging sensor plane of a high-speed camera after passing through the test section where blast wave develops. Compared to other Shadowgraph imaging system using white light, this system is easy to setup and adjust the illumination intensities. The disadvantage of using a laser in Shadowgraph or Schlieren is that the image is prone to be contaminated by the interference pattern [10]. The field of view is of 35 cm in diameter, so that the tissue sample and the blast wave can be fully illuminated. A high speed CMOS camera (Phantom v7.3) can be operated at a maximum frame rate of 500,000 frames per second (fps). The sensor plane is of a physical dimension of  $17.6 \times 13.2 \text{ mm}^2$  and a maximum resolution  $800 \times 600 \text{ pixels}^2$  at 14-bit depth. In our experiment, the camera is operated at 90,000 fps and resolution of  $128 \times 128 \text{ pixels}^2$ .

One is reminded that there is a tradeoff between the

shadowgraph effect and the sharpness of the image as detailed in [10]. In the present experiment, we first use the imaging system to record shadowgraph images of the air-flow from a compressed air duster, and an optimal combination of the two collimating lenses is explored in order to obtain a balance between these two effects, before the system is finally used to record the images discussed in this paper. Also, since the blast event is hard to control, the camera started recording prior to the explosion. In this way, the entire development of blast wave can be recorded in middle of the image sequence. The valid image sequence containing the blast wave is selected in post-processing stage for analysis.

## RESULTS

Figure 2 gives a typical sequence of shadowgraph images showing the temporal development of blast wave structures, in which the blast wave evolves freely, i.e., no blockage of tissue sample and loading plate from underneath. The black rectangular zone in figure 2, image of the blast nozzle exit, gives a reference length scale of 6.4 mm. One can differentiate the start and development of blast wave, its decaying, and its dissipation from these images. In the development stage ( $t < 34 \mu\text{s}$ ), the wavefront displays good symmetry. The grayscale of the images along a vertical central line are chosen to locate and track the position of the blast wavefront, as indicated in figure 3, by locating the maximum change of grayscale (density). The displacement-versus-time history of the blast wavefront can then be used to estimate the propagation velocity, i.e.,  $V \sim \delta x / \delta t$ . The blast wave propagates at an estimated

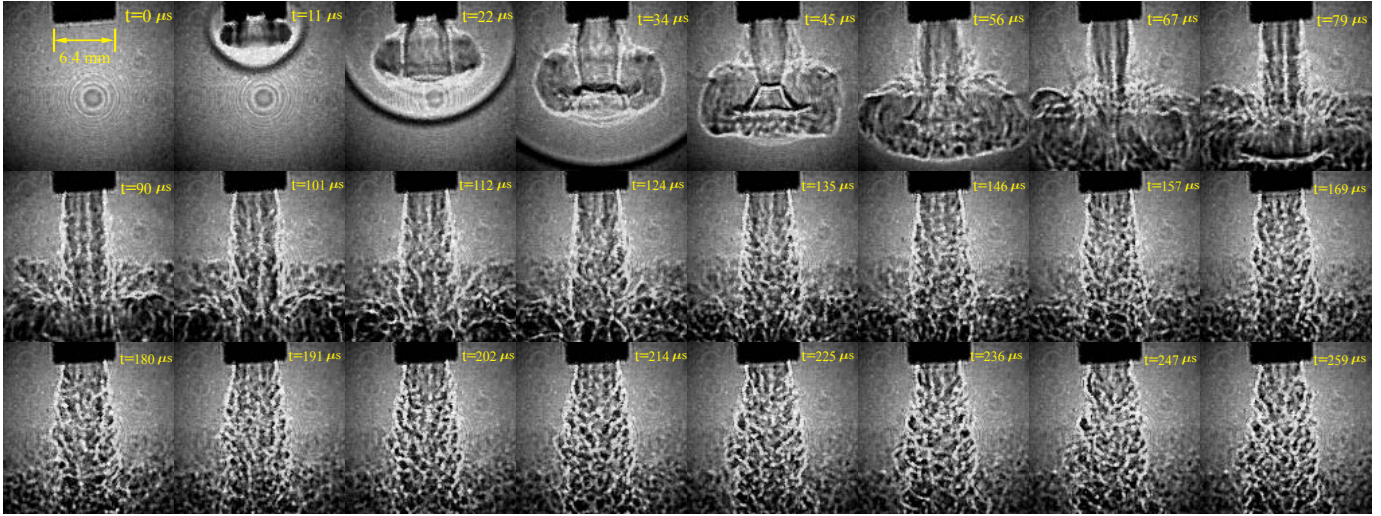


Figure 2. Shadowgraph Image sequence of free evolution of the blast wave.

peak Mach number of  $Ma \sim 1.31$  ( $V \sim 445$  m/s). One is

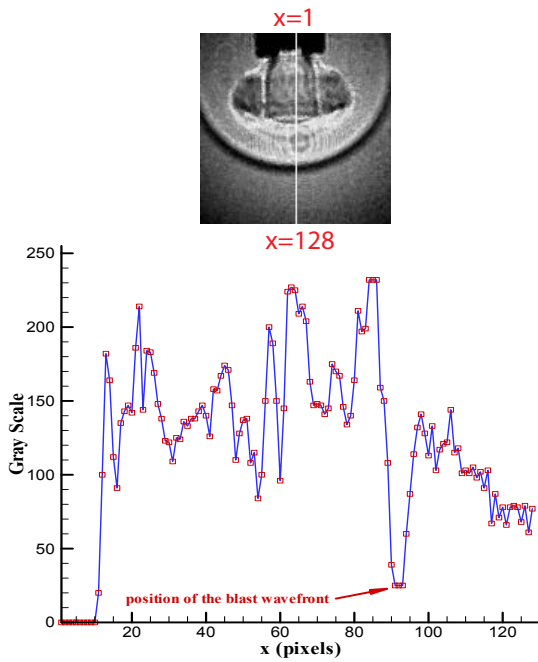


Figure 3. Grayscale information along a selected (white) line is analyzed to estimate the speed of blast wavefront.

reminded that the temporal evolution of the pressure is also of keen interest. The blast front causes an enormous rise in ambient pressure (over-pressure). As explosive gases

continue to expand from their point of origin, a negative under-pressure occurs after the positive over-pressure. The combination of this over-pressure and under-pressure can result in severe PBI [12]. As one of the on-going efforts, we are incorporating a high-speed pressure measurement system into the present setup, which is capable of giving a sequence of pressure measurement synchronized with high-speed shadowgraph.

The evolution of the blast wave correlated with loading applied on the spinal cord tissue and the deformation of the tissue is shown in figure 4. The deformation of tissue sample is extracted from the image. A relative deformation is defined as

$$\varepsilon = \frac{\delta H}{H_0}, \quad (2)$$

where the deformation is

$$\delta H = H - H_0. \quad (3)$$

$H$  is the mean height of a 8 mm central region of the tissue sample, as shown in figure 4.  $H_0$  is the original height of the tissue prior to blast impact. In this analysis, we assume that the tissue surface undergoes uniform deformation, which is characterized by  $\Delta H$  and  $\varepsilon$ . The surface of the tissue becomes less smooth in figure 4(7-9), and the

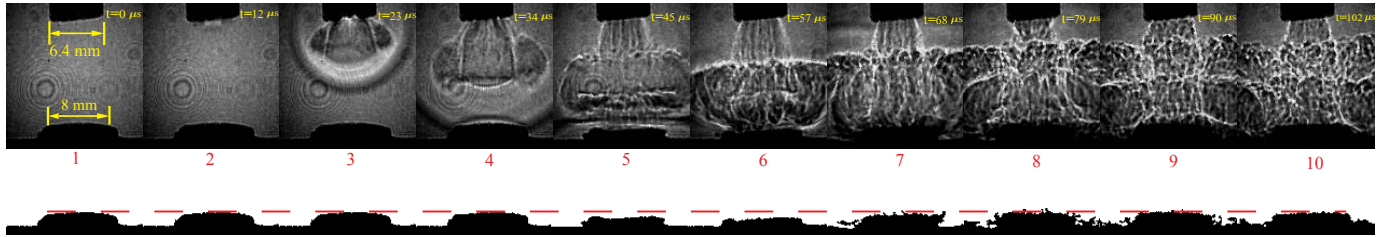


Figure 4. Interaction of blast wave and the spinal cord tissue sample (top) and corresponding deformation of tissue sample (bottom).

heights of the tissue at these instants are obtained by averaging over the 8 mm central region. The shape of the spinal cord seems to remain intact when the blast impacts on it (figure 4-4) and reflection on the tissue surface can be clearly observed in figure 4(4-5). After that the tissue is compressed ( $t = 45 \sim 57 \mu\text{s}$ , figure 4(5-6)), a severe deformation is observed at the enter of the tissue sample. Then, in the following  $40 \mu\text{s}$ , the tissue sample restores from the severe deformation. The development of relative deformation, as a function of time, is shown in figure 5. The surface deformation rate can then be estimated by  $v = \delta H / \delta t$ . The averaged surface deformation rate during the loading process (squeezing) is 31.3 m/s, and the one corresponding to the unloading process (recovering) is 15.7 m/s. So the loading and unloading under blast impact is a super-fast event, which presents a major challenge for model simulation to reveal the internal stress/strain distribution within the sample body. The measured surface deformation is used as realistic boundary conditions in numerical simulation (ongoing effort) for examining the stress distribution, which will further identify regions of PBI.

## SUMMARY

A high-speed imaging system is used, together with a laser-based shadowgraph technique, to visualize the propagation of the blast wave and the impact with spinal cord tissue in a miniature *ex vivo* BINT model. The set-up allows for rapid characterization of the physical mechanisms responsible for BINT. The development of the blast wave structure and the resultant deformation of the spinal cord tissue are characterized. Propagation velocity of the blast wavefront is estimated from the shadowgraph images, also extracted are relative deformation and deformation rate of the tissue samples. The blast wave generated by the BINT model reaches a Mach number of 1.31. The surface defor-

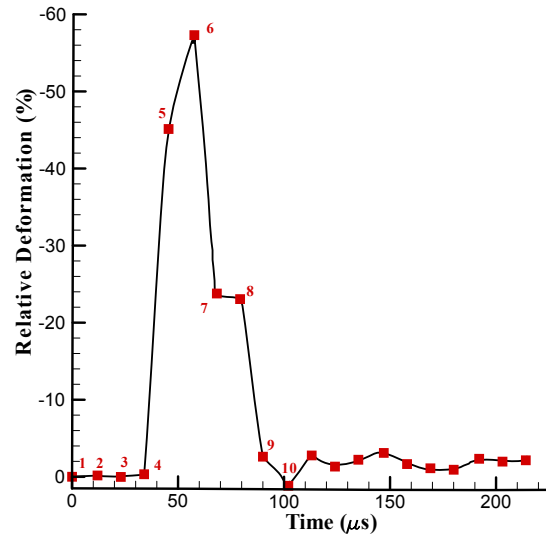


Figure 5. Relative deformation of the tissue sample as a function of time. The number labels correspond to the events in figure 4.

mation rates at loading and unloading processes are estimated of 31.3 m/s and 15.7 m/s, respectively. These measurements provide needed realistic boundary conditions for model simulations to reveal the internal stress distribution, which helps to identify the onset and development of PBI.

Ongoing efforts including correlating a high-frequency pressure measurement with the development of the blast wave, to identify events of over-pressure and under-pressure, and developing a numerical simulation model for investigating the internal stress distribution by applying the measured surface deformation as realistic boundary condition, as well as exploring the BINT mechanism by varying the intensity of the generated blast waves.

## REFERENCES

- [1] Bell, R., Vo, A., Neal, C., Tigno, J., Roberts, R., Mossop, C., Dunne, J., and Armonda, R., 2009. "Mil-

- itary traumatic brain and spinal column injury: a 5-year study of the impact blast and other military grade weaponry on the central nervous system”. *J. Trauma*, **66**, pp. S104–111.
- [2] Cernak, I., Wang, Z., Jiang, J., Bian, X., and Savic, J., 2001. “Ultrastructural and functional characteristics of blast injury-induced neurotrauma”. *J. Trauma*, **50**, pp. 695–706.
- [3] Kaur, C., Singh, J., Lim, M., Ng, B., Yap, E., and Ling, E., 1995. “The response of neurons and microglia to blast injury in the rat brain”. *Neuropathol. Appl. Neurobiol.*, **21**, pp. 369–377.
- [4] Cernak, I., Wang, Z., Jiang, J., Bian, X., and Savic, J., 2001. “Cognitive deficits following blast injury-induced neurotrauma: possible involvement of nitric oxide”. *Brain Inj.*, **15**, pp. 593–612.
- [5] Long, J., Bentley, T., Wessner, K., Cerone, C., Sweeney, S., and Bauman, R., 2009. “Blast overpressure in rats: Recreating a battlefield injury in the laboratory”. *J. Neurotrauma*, **26**, pp. 827–840.
- [6] LaPlaca, M., Lee, V., and Thibault, L., 1997. “An in vitro model of traumatic neuronal injury: loading rate-dependent changes in acute cytosolic calcium and lactate dehydrogenase release”. *J. Neurotrauma*, **14**, pp. 355–368.
- [7] LaPlaca, M., and Thibault, L., 1997. “An in vitro traumatic injury model to examine the response of neurons to a hydrodynamically-induced deformation”. *Ann Biomed Eng.*, **25**, pp. 665–677.
- [8] Ouyang, H., Galle, B., Li, J., Nauman, E., and Shii, R., 2008. “Critical roles of decompression in functional recovery of ex vivo spinal cord white matter”. *J. Neurotrauma*, **25**, pp. 19–29.
- [9] Ouyang, H., Galle, B., Li, J., Nauman, E., and Shii, R., 2009. “Biomechanics of spinal cord injury: a multimodal investigation using ex vivo guinea pig spinal cord white matter”. *J. Neurosurg Spine*, **10**, pp. 161–170.
- [10] Settles, G. S., 2001. *Schlieren and Shadowgraph Techniques*. Springer-Verlag Press, Germany.
- [11] Tropea, C., Yarin, A. L., and Foss, J. F., 2007. *Springer Handbook of Experimental Fluid Mechanics*. Springer-Verlag Berlin Heidelberg, Germany.
- [12] DePalma, R. G., Burris, D. G., Champion, H. R., and Hodgson, M. J., 2005. “Blast injuries”. *N. Engl. J. Med.*, **352**, pp. 1335–1342.